

Arrested Phase Separation in Double-Exchange Models: Large-Scale Simulation Enabled by Machine Learning

Puhan Zhang  and Gia-Wei Chern

Department of Physics, University of Virginia, Charlottesville, Virginia 22904, USA

 (Received 7 May 2021; accepted 8 September 2021; published 29 September 2021)

We present large-scale dynamical simulations of electronic phase separation in the single-band double-exchange model based on deep-learning neural-network potentials trained from small-size exact diagonalization solutions. We uncover an intriguing correlation-induced freezing behavior as doped holes are segregated from half filled insulating background during equilibration. While the aggregation of holes is stabilized by the formation of ferromagnetic clusters through Hund's coupling between charge carriers and local magnetic moments, this stabilization also creates confining potentials for holes when antiferromagnetic spin-spin correlation is well developed in the background. The dramatically reduced mobility of the self-trapped holes prematurely disrupts further growth of the ferromagnetic clusters, leading to an arrested phase separation. Implications of our findings for phase separation dynamics in materials that exhibit colossal magnetoresistance effect are discussed.

DOI: [10.1103/PhysRevLett.127.146401](https://doi.org/10.1103/PhysRevLett.127.146401)

The subject of phase separation dynamics is of significant importance in many branches of physics, materials science, and biology [1–5]. Dynamically, phase separation occurs when a homogeneous system is placed in an out-of-equilibrium state due to a rapid change in thermodynamic variables, such as temperature. The system then evolves toward an inhomogeneous state of coexisting phases. This intrinsically nonequilibrium and nonlinear process involves the formation, growth, and coarsening of domains of ordered phases. Substantial progress has been made in understanding the phase separation kinetics over the past few decades. In particular, it has been shown that phase separation at late times exhibits a dynamical scaling and is controlled by a characteristic length scale L , which follows a power law $L(t) \sim t^\alpha$, where the growth exponent α depends mainly on dimensionality and conservation of the order parameter.

Phase separation also plays a crucial role in the functionality of strongly correlated electron systems [6–17]. A case in point is the complex inhomogeneous states observed in manganites and magnetic semiconductors that exhibit the colossal magnetoresistance (CMR) effect [12–17]. These nanoscale textures arise from the segregation of hole-rich ferromagnetic clusters from the half filled antiferromagnetic domains [18–20]. An intriguing scenario for CMR is the field-induced percolating transition of metallic nanoclusters in such a phase-separated state [21,22]. Because the number of doped carriers is conserved, the segregation process of such conserved field was first studied in the classic works of Lifshitz and Slyozov [23] and Wagner [24] (LSW), who predicted a growth exponent of $\alpha = 1/3$.

Despite extensive works on properties of mixed-phase states in CMR materials, the kinetics of phase separation driven by electron correlation has yet to be investigated. Important questions, such as whether the phase separation exhibits dynamical scaling and does the late-stage domain growth indeed follow the LSW power law, remain unanswered. On the theoretical side, the lack of progress is partially due to the difficulty in performing large-scale dynamical simulations of electronic phase separation. While several numerical techniques, such as molecular dynamics and the phase-field method [25–27], have been developed to simulate pattern formation in material systems such as binary alloys or polymers, conventional approaches often rely on empirical energy models and cannot describe the intricate electron correlation effects. A comprehensive modeling of correlation-induced phase separation requires properly incorporating microscopic electronic processes into mesoscopic spatial-temporal pattern dynamics. Yet, such multiscale approaches are limited to small systems due to the expensive repeated electronic structure calculations.

In this Letter, we overcome the difficulties of multiscale modeling by applying machine-learning (ML) methods to enable large-scale simulations of phase separation phenomena in the double-exchange (DE) model [28–30], which plays a center role in the modeling of CMR materials. The central idea of our approach is to develop deep-learning neural networks (NNs) that emulate the time-consuming exact diagonalization required for computing the exchange forces on spins. In this respect, the NNs can be viewed as a complex empirical potential model, which offers the accuracy of quantum calculations. We consider the single-band DE model on a square lattice,

$$\hat{\mathcal{H}} = -t_{\text{nn}} \sum_{\langle ij \rangle} (\hat{c}_{i\alpha}^\dagger \hat{c}_{j\alpha} + \text{H.c.}) - J_H \sum_i \mathbf{S}_i \cdot \hat{c}_{i\alpha}^\dagger \boldsymbol{\sigma}_{\alpha\beta} \hat{c}_{i\beta}, \quad (1)$$

where $\hat{c}_{i\alpha}^\dagger/\hat{c}_{i,\alpha}$ are creation and annihilation operators, respectively, of electron with spin $\alpha = \uparrow, \downarrow$ at site i , H.c. stands for the Hermitian conjugate, repeated indices α, β implies spin summation, $\langle ij \rangle$ indicates the nearest-neighbor pairs, t_{nn} is the nearest-neighbor electron hopping constant, J_H is the local Hund's rule coupling between electron spin and local magnetic moment \mathbf{S}_i , which are assumed to be classical spins of length $S = 1$. The square-lattice DE model has been extensively studied theoretically [31–35]. In particular, when the system is slightly hole doped from half filling, a mixed-phase state consisting of hole-rich ferromagnetic puddles embedded in the half filled anti-ferromagnetic insulator emerges as a stable thermodynamic phase at strong Hund's coupling [32–34].

The evolution of the DE system in the adiabatic limit, similar to the Born-Oppenheimer approximation in quantum molecular dynamics [36], is governed by the stochastic Landau-Lifshitz-Gilbert (LLG) equation [37–39]

$$\frac{d\mathbf{S}_i}{dt} = \mathbf{S}_i \times (\mathbf{H}_i + \boldsymbol{\zeta}_i) - \alpha \mathbf{S}_i \times (\mathbf{S}_i \times \mathbf{H}_i), \quad (2)$$

where $\boldsymbol{\zeta}_i(t)$ is a Gaussian stochastic field of zero mean, α is a damping coefficient, and $\mathbf{H}_i = -\partial E/\partial \mathbf{S}_i$ is the local exchange force acting on the i th spin. The effective energy E is given by $E = \text{Tr}(\hat{\rho} \hat{\mathcal{H}})$, where $\hat{\rho} = \exp(-\hat{\mathcal{H}}/k_B T)$ is the instantaneous density matrix of the electron liquid. Repeated calculation of ρ , which is required at every time step, based on exact diagonalization (ED), can be overwhelmingly time consuming [40–46]. On the other hand, effective classical spin models for the DE Hamiltonian requires multiple many-spin interaction terms [47–49]. The determination of these coupling coefficients is numerically very challenging. Moreover, the error of the empirical expansion is not well controlled.

To overcome this computational bottleneck, we develop a NN model for the potential energy surface $E(\{\mathbf{S}_i\})$ of spins. We first express the effective energy as a sum of local contributions

$$E = \sum_i \epsilon_i = \sum_i \epsilon(\mathcal{C}_i), \quad (3)$$

where the energy $\epsilon_i = \epsilon(\mathcal{C}_i)$ is associated with the i th lattice site and is assumed to depend only on spin configuration $\mathcal{C}_i = \{\mathbf{S}_j | r_{ij} < r_c\}$ in its neighborhood. The partitioning of E into local energies is based on the locality principle [50,51], which also underlies the ML interatomic potentials that allow for large-scale molecular dynamics simulations with the accuracy of density-functional theory [52–59] or other many-body techniques [60–62].

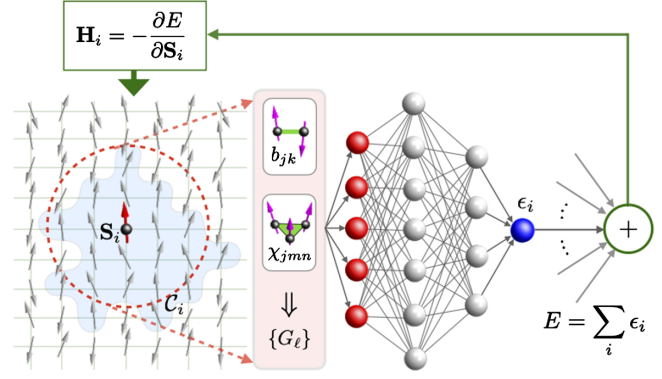


FIG. 1. Schematic diagram of neural-network (NN) potential model for LLG dynamics simulation of DE system. A descriptor generates the neighborhood spin configuration \mathcal{C}_i to effective coordinates $\{G_\ell\}$ which are then fed into a NN. The output of the NN is the local energy $\epsilon_i = \epsilon(\mathcal{C}_i)$ associated with site- i . Automatic differentiation applied to the total energy obtained from all sites gives the local exchange forces \mathbf{H}_i .

As shown in Fig. 1, the dependence of energy function $\epsilon(\mathcal{C}_i)$ on the local spin environment is encoded in a feed-forward neural network. To ensure that symmetries of the DE Hamiltonian, which are described by the $\text{SO}(3)$ spin-rotation and D_4 point groups, are preserved in the energy function, we have developed a descriptor that translates local spin configuration \mathcal{C}_i into effective coordinates $\{G_\ell\}$ that are invariant under both symmetry operations. First, the $\text{SO}(3)$ rotation symmetry can be manifestly maintained by using only bond variables b_{jk} and scalar chirality χ_{jmn} as building blocks; they are defined as

$$b_{jk} = \mathbf{S}_j \cdot \mathbf{S}_k, \quad \chi_{jmn} = \mathbf{S}_j \cdot \mathbf{S}_m \times \mathbf{S}_n. \quad (4)$$

The collection of these variables around the i th spin $\{b_{jk}, \chi_{jmn}\}$ form the basis of a high-dimensional representation of the D_4 group, which is then decomposed into the fundamental irreducible representations (IRs) [63]. The basis of each IR $f_r^{A_1}, f_r^{A_2}, \dots, f_r^E$, where r enumerates the multiplicity, is proper linear combinations of the bond and scalar chirality variables. Finally, generalized coordinates $\{G_\ell\}$ that are invariant under lattice symmetry operations are obtained from the amplitudes and relative phases of these IR basis [64]. More details can be found in the Supplemental Material [65]. These generalized coordinates are then fed into a NN, which produces the local energy ϵ_i at its output. Exchange forces \mathbf{H}_i acting on spins are obtained by applying automatic differentiation to the total energy; see Fig. 1.

A six-layer NN model is constructed and trained using PyTorch [65–71]. The training dataset consists of 3500 snapshots of spins and local exchange forces, obtained from exact LLG calculations of a 30×30 lattice; see Supplemental Material for details about the datasets [65]. Figure 2(a) shows components of local exchange

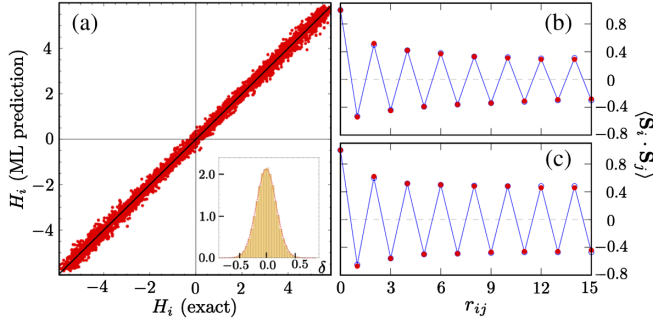


FIG. 2. (a) ML predicted exchange forces versus exact solutions from test dataset. The inset shows distribution of the force difference $\delta = H_{\text{ML}} - H_{\text{exact}}$ between ML prediction and ED, which is well approximated by a normal distribution, shown as the red line, with a variance $\sigma^2 = 0.035$. Right: spin-spin correlation $\langle \mathbf{S}_i \cdot \mathbf{S}_j \rangle$ as a function of $r_{ij} = |\mathbf{r}_j - \mathbf{r}_i|$ along the x direction at electron filling fraction (b) $n = 0.485$ and (c) $n = 0.475$. The red dots are results from LLG simulations with NN models *without* the Langevin noise, while the blue lines correspond to ED-LLG simulations at $T = 0.022$.

forces \mathbf{H}_i predicted by our trained NN model versus the exact results on test datasets. The difference $\delta = H_{\text{ML}} - H_{\text{exact}}$ is well described by a Gaussian distribution with a rather small mean-square error of $\sigma^2 = 0.035$, as shown in the inset. Interestingly, the normal distribution of the deviation δ implies that the statistical error of the ML model can be interpreted as an effective or artificial temperature in Langevin dynamics. We next combine the trained NN model with the LLG dynamics to perform a quench simulation, in which random spins on a 30×30 lattice are quenched to a low temperature $T = 0.022$, which is also the temperature used to train the NN. The same simulations are then repeated using exact diagonalization. The spin-spin correlation functions obtained from the ML and ED-LLG simulations are shown in Figs. 2(b) and 2(c) for two different electron fillings. The nice agreements between the two methods further confirm the accuracy of force prediction and demonstrate the transferability of the NN model in dynamical simulations.

Having successfully benchmarked the NN model, we used it to perform large-scale quench simulations on a 100×100 system. Figure 3 shows density plots of local spin correlation obtained by averaging over four nearest-neighbor bonds of a given site, $b_i \equiv (\mathbf{S}_i \cdot \mathbf{S}_{i+x} + \mathbf{S}_i \cdot \mathbf{S}_{i-x} + \mathbf{S}_i \cdot \mathbf{S}_{i+y} + \mathbf{S}_i \cdot \mathbf{S}_{i-y})/4$, at different times after quench. Positive b_i corresponds to regions with predominantly ferromagnetic (FM) alignment of spins, while negative b_i indicates antiferromagnetic (AFM) domains. Our ML-LLG simulations clearly showed a relaxation process that leads to an inhomogeneous state with large AFM domains interspersed with small FM clusters. We have trained another NN model that successfully predicts the on-site electron density $n_i = \frac{1}{2} \sum_{\sigma} \langle \hat{c}_{i,\sigma}^\dagger \hat{c}_{i,\sigma} \rangle$ based on the neighborhood spins C_i .

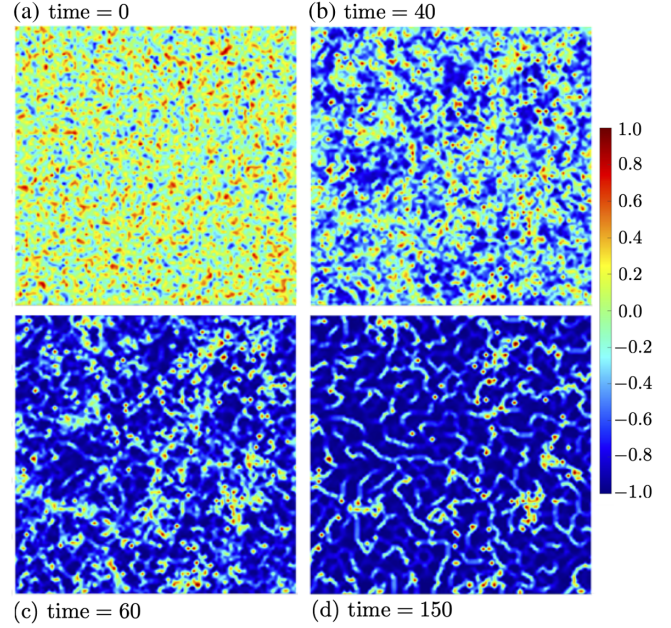


FIG. 3. Density plots of local bond variables $b(\mathbf{r}_i)$ at four different times [(a) time = 0, (b) time = 40, (c) time = 60 and (d) time = 150] of the ML-LLG dynamics simulation on a 100×100 lattice with 1.5% hole doping. The NN model is trained by datasets from exact solutions on a $L = 30$ lattice, with parameters $t_{\text{nn}} = 1$, $J_H = 7$, and electron filling fraction $n = 0.485$. The simulation time is measured in units of t_{nn}^{-1} .

Applying this NN to spin configurations obtained from the ML-LLG quench simulations, we verified that the doped holes are indeed confined to puddles with FM spins, as shown in Figs. 4(a) and 4(b). Interestingly, compared with the electron density, the spins exhibit more complex structures. In particular, in addition to FM clusters, a web of stringlike features can be seen in the AFM background of the phase-separated states; see, e.g., Fig. 3(d).

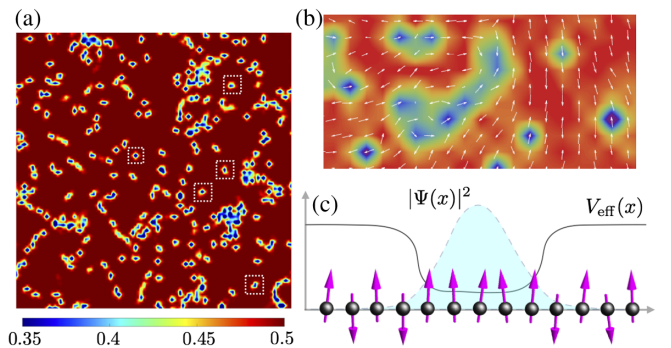


FIG. 4. (a) Density plot of on-site electron density n_i , predicted from NN models for the spin configuration shown in Fig. 3(d). Some magnetic polarons are highlighted by dotted squares. (b) A close-up look of the FM clusters and the accompanying spins (projected to a 2D plane). (c) Schematic diagram showing self-confinement of carriers in a FM cluster.

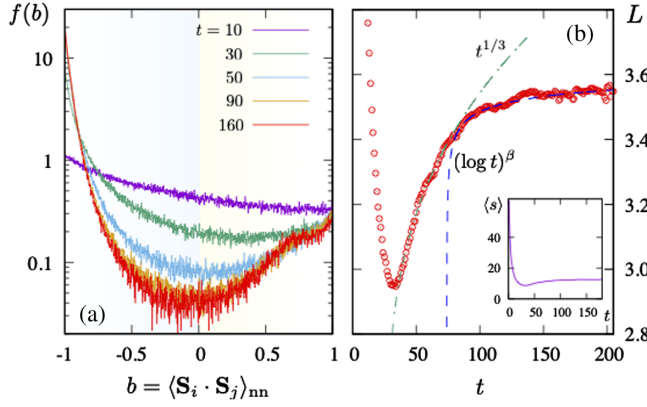


FIG. 5. (a) Distribution function of the nearest-neighbor bond-variables at different times during phase separation. (b) Average linear size $L = \langle s \rangle^{1/2}$ of FM clusters versus time after a thermal quench. The dash-dot line shows the $t^{1/3}$ power-law growth, while the dashed line indicates sublogarithmic dependence $L(t) \sim (\log t)^\beta$ with $\beta = 0.11$. The inset shows the time dependence of average size $\langle s \rangle$ of FM clusters.

Next we turn to the kinetics of FM domain growth. Figure 5(a) shows the distribution of nearest-neighbor bond-variable $b = \langle \mathbf{S}_i \cdot \mathbf{S}_j \rangle_{nn}$ at different times after quench. The initially flat distribution function $f(b) = 1/(b_{\max} - b_{\min}) = \frac{1}{2}$, corresponding to random spins, starts to develop a peak at $b_{\min} = -1$, representing AFM spin correlation at earlier times (e.g., at $t = 10$). This then turns into a bimodal distribution at late times, clearly indicating the evolution of the system toward phase separation, although the peak at the FM bond $b_{\max} = +1$ is rather weaker. Since doped holes in the phase-separated states are mostly confined in FM clusters, the smaller value of $f(b_{\max})$ is consistent with the small doping of our system.

We define a FM cluster in such a way that all nearest-neighbor bonds within it are greater than a threshold $b_{\text{th}} = 0.5$. The time dependence of the characteristic length L of such FM clusters is shown in Fig. 5(b). Qualitatively similar behaviors were obtained using larger threshold b_{th} . In the initial state with random spins, a fraction $\frac{1}{2}(1 - b_{\text{th}}) = \frac{1}{4}$ of bonds are above the threshold. Although this fraction is still below the bond-percolation threshold $p_{\text{th}} = 1/2$ on square lattice, relatively large FM clusters can still be found in random spins, which explains the initially large average size $\langle s \rangle$ of FM clusters. As the system relaxes toward equilibrium, the average size quickly decreases, as shown in the inset of Fig. 5(b). After reaching a minimum, the FM clusters start to grow again.

Since the number of doped holes is conserved, phenomenologically the growth of such conserved fields is described by the Cahn-Hilliard equation [72], also called the model-B dynamics [73], and a power-law growth $L(t) \sim t^{1/3}$ is expected. Moreover, since the density of doped holes is very small in the mixed-phase states, the phase separation dynamics in such asymmetric quenches is

supposed to be well described by the original LSW theory [23,24], which convincingly predicts the same $t^{1/3}$ growth. However, as shown in Fig. 5(b), only a short initial period of the domain growth can be described by the $\alpha = 1/3$ power law. At late times, the length scale L increases with a significantly slower rate than that predicted by the LSW theory.

The LSW theory describes the diffusive interactions between domains of conserved minority phase. Clusters of the minority phase compete for growth through an evaporation-condensation mechanism, whereby larger clusters grow at the expense of smaller ones. According to this scenario, the growth of the hole-rich FM cluster requires the migration of doped holes from smaller clusters to larger ones in the mixed-phase state. The initial aggregation of the charge carriers into proto-FM domains can probably be described by the LSW mechanism, as evidenced by the early stage power-law growth in our simulations. However, the phase separation process is dramatically slowed down when the AFM correlation is established in the background of the half filled majority phase. At this point, the doped holes induce a cloud of surrounding parallel spins through the double-exchange mechanism, which in turn provide a confining potential. Figure 4(b) shows examples of hole-rich FM clusters embedded in an AFM background, and the self-confinement of holes in such domains is schematically shown in Fig. 4(c). Importantly, as a result of such self-trapping, evaporation of doped holes from FM clusters is strongly suppressed, leading to the breakdown of the LSW mechanism.

Moreover, even if some charge carriers manage to escape confinement of the emerging FM clusters described above, they are soon transformed to relatively immobile quasi-particles called magnetic polarons [30,74–79], some of which are highlighted in Fig. 4(b). Magnetic polaron of the single-band DE model consists of as few as five parallel spins that trap exactly one fundamental electric charge [79]. In fact, magnetic polarons to some extent can be viewed simply as the smallest FM cluster [12].

Another mechanism for $L \sim t^{1/3}$ domain growth, proposed by Binder and Stauffer (BS) [80,81], is based on the Brownian motion and collision of the minority-phase droplets. For the single-band DE Hamiltonian studied in this Letter, the FM clusters, including magnetic polarons, are pretty much immobile up to temperatures close to the magnetic phase transition [77–79]. This indicates the BS scenario cannot produce a sustained domain growth in our case. On the other hand, taking into account the quantum nature of localized spins, it has been argued that diffusive motion of small magnetic polarons can be achieved through quantum tunneling [82–84] or large paramagnetic fluctuations [85,86]. For most CMR materials, however, such quantum tunneling is suppressed due to the large magnitude of local spins. At any rate, even with diffusive magnetic polarons, a consistent treatment of

tunneling-induced evaporation of holes is required in order to see whether the LSW scaling might be restored.

In CMR materials and magnetic semiconductors, the formation of FM clusters and magnetic polarons are accompanied by local lattice distortion and orbital ordering [12], both of which are expected to further stabilize the composite structure, thus reducing the mobility of charge carriers. Consequently, a similar freezing effect is likely to take place in the phase separation process of real materials. The presence of quenched disorder most likely enhances the glassy behaviors discussed above. For example, it has been shown that charge carriers can be trapped by impurities, forming bound magnetic polarons [87–89]. Other factors that affect the carrier mobility include hole concentration and external electric and magnetic fields. In particular, higher doping percentage could increase the overlap of the carrier wave function, thus enhancing the tunneling mobility.

The functionality of correlated electron materials, such as CMR manganites, depends intimately on the structure of the mixed-phase states, which, in turn, are determined by the phase separation process. Some reported anomalous or glassy dynamics in CMR manganites [90–92] might be related to the freezing behavior studied in this Letter. ML-enabled large-scale simulations offer the capability to systematically investigate and characterize phase separation dynamics, paving the way toward engineering electronic mixed-phase states with desired properties. With powerful ML methods, generalizations to more realistic models, which include, e.g., multiorbital or the Jahn-Teller effect, are now feasible. For example, the inclusion of a local Jahn-Teller distortion means that simultaneous quantum MD and LLG simulation is required for the dynamics of Jahn-Teller phonons and local spins, and a generalized NN model has to be developed that can predict forces for both degrees of freedom. Additional care has to be taken in the presence of crystallographic defects such as dislocations. The reduced or even absence of point group symmetry requires extra effort for the combined displacement–magnetic descriptors. The magnetic descriptor developed in this Letter, properly combined with descriptors developed for ML interatomic potential models [93,94], also has potential applications beyond lattice-based models, for example, LLG simulations of spin glasses and MD simulations with magnetic degrees of freedom.

The authors thank Sheng Zhang for useful discussions. The work was supported by the U.S. Department of Energy Basic Energy Sciences under Award No. DE-SC0020330. The authors acknowledge Research Computing at The University of Virginia for providing computational resources and technical support that have contributed to the results reported within this publication.

- [1] J. D. Gunton, M. San Miguel, and P. S. Saint, The dynamics of first order phase transitions, in *Phase Transitions and Critical Phenomena*, edited by C. Domb and J. L. Lebowitz (Academic, New York, 1983), Vol. 8, pp. 269–466.
- [2] A. J. Bray, Theory of phase-ordering kinetics, *Adv. Phys.* **43**, 357 (1994).
- [3] *Kinetics of Phase Transitions*, edited by S. Puri and V. Wadhawan (CRC Press, Taylor & Francis Group, London, 2009).
- [4] A. Onuki, *Phase Transition Dynamics* (Cambridge University Press, Cambridge, England, 2002).
- [5] M. Cross and H. Greenside, *Pattern Formation and Dynamics in Nonequilibrium Systems* (Cambridge University Press, Cambridge, England, 2012).
- [6] H. J. Schulz, Domain walls in a doped antiferromagnet, *J. Phys. II (France)* **50**, 2833 (1989).
- [7] V. J. Emery, S. A. Kivelson, and H. Q. Lin, Phase Separation in the $t - J$ Model, *Phys. Rev. Lett.* **64**, 475 (1990).
- [8] S. White and D. Scalapino, Phase separation and stripe formation in the two-dimensional $t - J$ model: A comparison of numerical results, *Phys. Rev. B* **61**, 6320 (2000).
- [9] J. M. Tranquada, B. J. Sternlieb, J. D. Axe, Y. Nakamura, and S. Uchida, Evidence for stripe correlations of spins and holes in copper oxide superconductors, *Nature (London)* **375**, 561 (1995).
- [10] S. A. Kivelson, I. P. Bindloss, E. Fradkin, V. Oganesyan, J. M. Tranquada, A. Kapitulnik, and C. Howald, How to detect fluctuating stripes in the high-temperature superconductors, *Rev. Mod. Phys.* **75**, 1201 (2003).
- [11] C.-H. Yee and L. Balents, Phase Separation in Doped Mott Insulators, *Phys. Rev. X* **5**, 021007 (2015).
- [12] E. Dagotto, *Nanoscale Phase Separation and Colossal Magnetoresistance* (Springer, Berlin, 2002).
- [13] E. Dagotto, Complexity in strongly correlated electronic systems, *Science* **309**, 257 (2005).
- [14] A. Moreo, S. Yunoki, and E. Dagotto, Phase separation scenario for manganese oxides and related materials, *Science* **283**, 2034 (1999).
- [15] E. Dagotto, T. Hotta, and A. Moreo, Colossal magnetoresistant materials: The key role of phase separation, *Phys. Rep.* **344**, 1 (2001).
- [16] N. Mathur and P. Littlewood, Mesoscopic texture in manganites, *Phys. Today* **56**, No. 1, 25 (2003).
- [17] E. L. Nagaev, *Colossal Magnetoresistance and Phase Separation in Magnetic Semiconductors* (Imperial College Press, London, 2002).
- [18] M. Fäth, S. Freisem, A. A. Menovsky, Y. Tomioka, J. Aarts, and J. A. Mydosh, Spatially inhomogeneous metal-insulator transition in doped manganites, *Science* **285**, 1540 (1999).
- [19] M. B. Salamon and M. Jaime, The physics of manganites: Structure and transport, *Rev. Mod. Phys.* **73**, 583 (2001).
- [20] Ch. Renner, G. Aeppli, B.-G. Kim, Y.-A. Soh, and S.-W. Cheong, Atomic-scale images of charge ordering in mixed-valence manganite, *Nature (London)* **416**, 518 (2002).
- [21] M. Uehara, S. Mori, C. H. Chen, and S.-W. Cheong, Percolative phase separation underlies colossal magnetoresistance in mixed-valent manganites, *Nature (London)* **399**, 560 (1999).

- [22] L. Zhang, C. Israel, A. Biswas, R. L. Greene, and A. de Lozanne, Direct observation of percolation in a maganite thin film, *Science* **298**, 805 (2002).
- [23] I. M. Lifshitz and V. V. Slyozov, The kinetics of precipitation from supersaturated solid solutions, *J. Phys. Chem. Solids* **19**, 35 (1961).
- [24] C. Wagner, Theorie der Alterung von Niederschlagen durch Umlosen, *Z. Elektrochem.* **65**, 581 (1961).
- [25] J. B. Collins and H. Levine, Diffuse interface model of diffusion-limited crystal growth, *Phys. Rev. B* **31**, 6119(R) (1985).
- [26] O. T. Valls and G. F. Mazenko, Nucleation in a time-dependent Ginzburg-Landau model: A numerical study, *Phys. Rev. B* **42**, 6614 (1990).
- [27] I. Steinbach, Phase-field model for microstructure evolution at the mesoscopic scale, *Annu. Rev. Mater. Res.* **43**, 89 (2013).
- [28] C. Zener, Interaction between the d -shells in the transition metals. II. Ferromagnetic compounds of manganese with perovskite structure, *Phys. Rev.* **82**, 403 (1951).
- [29] P. W. Anderson and H. Hasegawa, Considerations on double exchange, *Phys. Rev.* **100**, 675 (1955).
- [30] P.-G. de Gennes, Effects of double exchange in magnetic crystals, *Phys. Rev.* **118**, 141 (1960).
- [31] C. M. Varma, Electronic and magnetic states in the giant magnetoresistive compounds, *Phys. Rev. B* **54**, 7328 (1996).
- [32] S. Yunoki, J. Hu, A. L. Malvezzi, A. Moreo, N. Furukawa, and E. Dagotto, Phase Separation in Electronic Models for Manganites, *Phys. Rev. Lett.* **80**, 845 (1998).
- [33] E. Dagotto, S. Yunoki, A. L. Malvezzi, A. Moreo, J. Hu, S. Capponi, D. Poilblanc, and N. Furukawa, Ferromagnetic Kondo model for manganites: Phase diagram, charge segregation, and influence of quantum localized spins, *Phys. Rev. B* **58**, 6414 (1998).
- [34] A. Chatopadhyay, A. J. Millis, and S. Das Sarma, $T = 0$ phase diagram of the double-exchange model, *Phys. Rev. B* **64**, 012416 (2001).
- [35] D. Pekker, S. Mukhopadhyay, N. Trivedi, and P. M. Goldbart, Double-exchange model for noninteracting electron spins coupled to a lattice of classical spins: Phase diagram at zero temperature, *Phys. Rev. B* **72**, 075118 (2005).
- [36] D. Marx and J. Hutter, *Ab Initio Molecular Dynamics: Basic Theory and Advanced Methods* (Cambridge University Press, Cambridge, England, 2009).
- [37] L. D. Landau and E. M. Lifshitz, On the theory of the dispersion of magnetic permeability in ferromagnetic bodies, *Z. Phys.* **8**, 153 (1935).
- [38] W. F. Brown, Jr., Thermal fluctuations of a single-domain particle, *Phys. Rev.* **130**, 1677 (1963).
- [39] D. A. Garanin, Fokker-Planck and Landau-Lifshitz-Bloch equations for classical ferromagnetism, *Phys. Rev. B* **55**, 3050 (1997).
- [40] Linear-scaling approaches, such as the kernel polynomial method, have also been developed for the simulating DE systems; See Refs. [41–46] for examples. The ML approaches proposed in this Letter offer more flexibility and can be generalized to include effects such as multiorbitals, Jahn-Teller coupling, without much overhead.
- [41] N. Furukawa and Y. Motome, Order N Monte Carlo algorithm for fermion systems coupled with fluctuating adiabatical fields, *J. Phys. Soc. Jpn.* **73**, 1482 (2004).
- [42] G. Alvarez, C. Sen, N. Furukawa, Y. Motome, and E. Dagotto, The truncated polynomial expansion Monte Carlo method for fermion systems coupled to classical fields: A model independent implementation, *Comput. Phys. Commun.* **168**, 32 (2005).
- [43] A. Weisse, G. Wellein, A. Alvermann, and H. Fehske, The Kernel polynomial method, *Rev. Mod. Phys.* **78**, 275 (2006).
- [44] K. Barros and Y. Kato, Efficient Langevin simulation of coupled classical fields and fermions, *Phys. Rev. B* **88**, 235101 (2013).
- [45] G.-W. Chern, K. Barros, Z. Wang, H. Suwa, and C. D. Batista, Semiclassical dynamics of spin density waves, *Phys. Rev. B* **97**, 035120 (2018).
- [46] Z. Wang, G.-W. Chern, C. D. Batista, and K. Barros, Gradient-based stochastic estimation of the density matrix, *J. Chem. Phys.* **148**, 094107 (2018).
- [47] A. A. Caparica, A. Bunker, and D. P. Landau, Classical ferromagnet with double-exchange interaction: High-resolution Monte Carlo simulations, *Phys. Rev. B* **62**, 9458 (2000).
- [48] Y. Akagi, M. Udagawa, and Y. Motome, Hidden Multiple-Spin Interactions as an Origin of Spin Scalar Chiral Order in Frustrated Kondo Lattice Models, *Phys. Rev. Lett.* **108**, 096401 (2012).
- [49] H. Ishizuka and Y. Motome, Strong coupling theory for electron-mediated interactions in double-exchange models, *Phys. Rev. B* **92**, 024415 (2015).
- [50] K. Walter, Density Functional and Density Matrix Method Scaling Linearly with the Number of Atoms, *Phys. Rev. Lett.* **76**, 3168 (1996).
- [51] E. Prodan and K. Walter, Nearsightedness of electronic matter, *Proc. Natl. Acad. Sci. U.S.A.* **102**, 11635 (2005).
- [52] J. Behler and M. Parrinello, Generalized Neural-Network Representation of High-Dimensional Potential-Energy Surfaces, *Phys. Rev. Lett.* **98**, 146401 (2007).
- [53] A. P. Bartók, M. C. Payne, R. Kondor, and G. Csányi, Gaussian Approximation Potentials: The Accuracy of Quantum Mechanics, Without the Electrons, *Phys. Rev. Lett.* **104**, 136403 (2010).
- [54] Z. Li, J. R. Kermode, and A. De Vita, Molecular Dynamics with On-the-Fly Machine Learning of Quantum-Mechanical Forces, *Phys. Rev. Lett.* **114**, 096405 (2015).
- [55] J. S. Smith, O. Isayev, and A. E. Roitberg, ANI-1: An extensible neural network potential with DFT accuracy at force field computational cost, *Chem. Sci.* **8**, 3192 (2017).
- [56] L. Zhang, J. Han, H. Wang, R. Car, and Weinan E, Deep Potential Molecular Dynamics: A Scalable Model with the Accuracy of Quantum Mechanics, *Phys. Rev. Lett.* **120**, 143001 (2018).
- [57] J. Behler, Perspective: Machine learning potentials for atomistic simulations, *J. Chem. Phys.* **145**, 170901 (2016).
- [58] V. L. Deringer, M. A. Caro, and G. Csányi, Machine learning interatomic potentials as emerging tools for materials science, *Adv. Mater.* **31**, 1902765 (2019).
- [59] T. Mueller, A. Hernandez, and C. Wang, Machine learning for interatomic potential models, *J. Chem. Phys.* **152**, 050902 (2020).
- [60] R. T. McGibbon, A. G. Taube, A. G. Donchev, K. Siva, F. Hernández, C. Hargus, K.-H. Law, J. L. Klepeis, and D. E. Shaw, Improving the accuracy of Moller-Plesset

- perturbation theory with neural networks, *J. Chem. Phys.* **147**, 161725 (2017).
- [61] S. Chmiela, A. Tkatchenko, H. E. Sauceda, I. Poltavsky, K. T. Schütt, and K.-R. Müller, Machine learning of accurate energy-conserving molecular force fields, *Sci. Adv.* **3**, e1603015 (2017).
- [62] H. Suwa, J. S. Smith, N. Lubbers, C. D. Batista, G.-W. Chern, and K. Barros, Machine learning for molecular dynamics with strongly correlated electrons, *Phys. Rev. B* **99**, 161107(R) (2019).
- [63] M. Mameresh, *Group Theory and Its Application to Physical Problems* (Dover, New York, 1962).
- [64] J. Ma, P. Zhang, Y. Tan, A. W. Ghosh, and G.-W. Chern, Machine learning electron correlation in a disordered medium, *Phys. Rev. B* **99**, 085118 (2019).
- [65] See Supplemental Material at <http://link.aps.org/supplemental/10.1103/PhysRevLett.127.146401> for more details about the descriptor, in particular, the group-theoretical methods for constructing invariants of the point group, machine-learning techniques related to our work, and training details including dataset selection and loss function, which also includes Refs. [66–71].
- [66] A. Paszke, S. Gross, F. Massa, A. Lerer, J. Bradbury, G. Chanan, T. Killeen, Z. Lin, N. Gimelshein, L. Antiga, and A. Desmaison, PyTorch: An imperative style, high-performance deep learning library, in *Advances in Neural Information Processing Systems* (NeurIPS (Neural Information Proceeding Systems), San Diego, 2019), pp. 8024–8035.
- [67] V. Nair and G. E. Hinton, in *Proceedings of the 27th International Conference on International Conference on Machine Learning, ICML'10* (Omnipress, Madison, 2010), pp. 807–814.
- [68] J. Barron, Continuously differentiable exponential linear units, [arXiv:1704.07483](https://arxiv.org/abs/1704.07483).
- [69] A. Paszke, S. Gross, S. Chintala, G. Chanan, E. Yang, Z. DeVito, Z. Lin, A. Desmaison, L. Antiga, and A. Lerer, Automatic differentiation in PyTorch, in *31st Conference on Neural Information Processing Systems (NIPS 2017)*, Long Beach, CA, USA (NeurIPS (Neural Information Proceeding Systems), San Diego, 2017).
- [70] K. He, X. Zhang, S. Ren, and J. Sun. Delving deep into rectifiers: Surpassing human-level performance on imagenet classification, in *Proceedings of the IEEE International Conference on Computer Vision* (IEEE, Piscataway, 2015), pp. 1026–1034.
- [71] D. P. Kingma and J. Ba, Adam: A method for stochastic optimization, [arXiv:1412.6980](https://arxiv.org/abs/1412.6980).
- [72] J. W. Cahn and J. E. Hilliard, Free energy of a nonuniform system. I. Interfacial free energy, *J. Chem. Phys.* **28**, 258 (1958).
- [73] P. C. Hohenberg and B. I. Halperin, Theory of dynamic critical phenomena, *Rev. Mod. Phys.* **49**, 435 (1977).
- [74] T. Kasuya and A. Yanase, Anomalous transport phenomena in Eu-chalcogenide alloys, *Rev. Mod. Phys.* **40**, 684 (1968).
- [75] E. L. Nagaev, Spin polaron theory for magnetic semiconductors with narrow bands, *Phys. Status Solidi B* **65**, 11 (1974).
- [76] A. Mauger, Magnetic polaron: Theory and experiment, *Phys. Rev. B* **27**, 2308 (1983).
- [77] M. Daghofer, W. Koller, H. G. Evertz, and W. von der Linden, Polaronic aspects of the two-dimensional ferromagnetic Kondo model, *J. Phys. Condens. Matter* **16**, 5469 (2004).
- [78] V. M. Pereira, J. Lopes dos Santos, and A. H. Castro Neto, Double exchange model at low densities: Magnetic polarons and Coulomb suppressed phase separation, [arXiv:0804.3094](https://arxiv.org/abs/0804.3094).
- [79] J. Luo and G.-W. Chern, Dynamics of electronically phase-separated states in the double exchange model, *Phys. Rev. B* **103**, 115137 (2021).
- [80] K. Binder and D. Stauffer, Theory for the Slowing down of the Relaxation and Spinodal Decomposition of Binary Mixtures, *Phys. Rev. Lett.* **33**, 1006 (1974).
- [81] K. Binder, Theory for the dynamics of “clusters.” II. Critical diffusion in binary systems and the kinetics of phase separation, *Phys. Rev. B* **15**, 4425 (1977).
- [82] G. Kemeny and S. D. Mahanti, Theory of rate processes and the compensation rule, *Proc. Natl. Acad. Sci. U.S.A.* **72**, 999 (1975).
- [83] N. L. Huang Liu and D. Emin, Double Exchange and Small-Polaron Hopping in Magnetic Semiconductors, *Phys. Rev. Lett.* **42**, 71 (1979).
- [84] A. S. Ioselevich, Spin Polarons and Variable Range Hopping in Magnetically Disordered Systems, *Phys. Rev. Lett.* **71**, 1067 (1993).
- [85] M. J. Calderon, L. Brey, and P. B. Littlewood, Stability and dynamics of free magnetic polarons, *Phys. Rev. B* **62**, 3368 (2000).
- [86] L. G. L. Wegener and P. B. Littlewood, Fluctuation-induced hopping and spin-polaron transport, *Phys. Rev. B* **66**, 224402 (2002).
- [87] T. Dietl and J. Spalek, Effect of thermodynamic fluctuations of magnetization on the bound magnetic polaron in dilute magnetic semiconductors, *Phys. Rev. B* **28**, 1548 (1983).
- [88] L. R. Ram-Mohan and P. A. Wolff, Energetics of acceptor-bound magnetic polarons in diluted magnetic semiconductors, *Phys. Rev. B* **38**, 1330 (1988).
- [89] A. Kaminski and S. Das Sarma, Magnetic and transport percolation in diluted magnetic semiconductors, *Phys. Rev. B* **68**, 235210 (2003).
- [90] Z. B. Yan and J.-M. Liu, Anomalous phase separation in $\text{La}_{0.225}\text{Pr}_{0.4}\text{Ca}_{0.375}\text{MnO}_3$: Consequence of temperature and magnetic-field cycles, *Appl. Phys. A* **104**, 471 (2011).
- [91] T. Z. Ward, Z. Gai, H. W. Guo, L. F. Yin, and J. Shen, Dynamics of a first-order electronic phase transition in manganites, *Phys. Rev. B* **83**, 125125 (2011).
- [92] W. Kundhikanjana, Z. Sheng, Y. Yang, K. Lai, E. Y. Ma, Y.-T. Cui, M. A. Kelly, M. Nakamura, M. Kawasaki, Y. Tokura, Q. Tang, K. Zhang, X. Li, and Z.-X. Shen, Direct Imaging of Dynamic Glassy Behavior in a Strained Manganite Film, *Phys. Rev. Lett.* **115**, 265701 (2015).
- [93] R. Kondor, A novel set of rotationally and translationally invariant features for images based on the non-commutative bispectrum, [arXiv:cs/0701127](https://arxiv.org/abs/cs/0701127).
- [94] A. P. Bartók, R. Kondor, and G. Csányi, On representing chemical environments, *Phys. Rev. B* **87**, 184115 (2013).